Energy Conversion and Management 166 (2018) 590–601

Contents lists available at ScienceDirect

Energy Conversion and Management

journal homepage: www.elsevier.com/locate/enconman

# Climatic behaviour of solar photovoltaic integrated with phase change material

Sourav Khanna[a,*], K.S. Reddy[b], Tapas K. Mallick[a,*]

[a] Environment and Sustainability Institute, Penryn Campus, University of Exeter, Cornwall TR10 9FE, United Kingdom
[b] Heat Transfer and Thermal Power Laboratory, Department of Mechanical Engineering, Indian Institute of Technology Madras, Chennai 600 036, India

ARTICLE INFO

*Keywords:*
Phase change material
Photovoltaic
Thermal management
Performance enhancement
Climate
Fins

ABSTRACT

In photovoltaic (PV) cells, a large portion of the solar-irradiance becomes heat which shoots the cell temperature up and decreases its electrical efficiency. The heat can be removed using phase-change-material (PCM) at the rear of the PV. In literature, the researchers have reported the performance of PV-PCM for their respective locations. However, selection criteria for climates suitable for PCM integration are not reported yet. Thus, it has been carried out in the current work. The model has been validated against the experimental measurements. It has been concluded that (i) the climates having less variations in the ambient temperature are more suitable for PCM integration. The electricity enhancement achieved by PV cooling is 9.7%. It reduces to 6.6% for the climate having large variations, (ii) Heat extraction by PCM-systems is more effective in warm climates in comparison to cold climates, (iii) PCM integration performs better in climates with low wind-speed, (iv) PCM is more effective for the climates where wind-flow is across the PV and (v) Climates having high solar-radiation is better for heat removal by PCM.

## 1. Introduction

Solar photovoltaic (PV) is one of the fastest growing renewable technologies. However, in PV cells, only a small portion of the solar irradiance manages to get transformed into electricity. The rest becomes heat and shoots the cell temperature up and, consequently, decreases its electrical efficiency [1]. The studies involving the use of phase change material (PCM) to cool the PV have been reviewed.

### 1.1. Experimental investigations

The works related to the experimental investigations of the PV-PCM system are as follows: Hasan et al. [2] have used five different PCMs: paraffin wax (RT20), capric–lauric acid (C–L), capric–palmitic acid (C–P), pure salt hydrate ($CaCl_2{\cdot}6H_2O$) and commercial blend (SP22) and found that the PV temperature can be reduced maximally by 18 °C for a solar flux of 1000 W/m$^2$. Indartono et al. [3] have shown the applicability of a petroleum jelly as PCM for the thermal management of the PV. Huang et al. [4] have introduced aluminium fins inside the PCM box to enhance the PV cooling and found a further reduction of 8 °C in the PV temperature. Hasan et al. [5] have studied the behaviour of the system in two climates: Dublin, Ireland and Vehari, Pakistan and found better performance at Vehari. Sharma et al. [6] have used the PCM for lowering down the temperature of building integrated concentrated PV and found 7.7% increment in the electricity. Cui et al. [7] have integrated the PCM with concentrated PV-thermoelectric system to enhance the system performance. Sardarabadi et al. [8] have pumped water through the tubes inside the PCM box to use the stored heat and reported a temperature drop of 16 °C in PV. Browne et al. [9] have also studied the utilization of the stored energy in the PCM by flowing water and reported a thermal efficiency of 20%. Huang et al. [10] have discussed the formation of the crystals in the PCM and its effect on the system performance. Researchers have reported the numerical investigations too to predict the system performance [11–14] which are presented in the subsequent sections.

### 1.2. Numerical investigations

There have been studies carrying out the one-dimensional thermal analysis of the PV-PCM system. The heat transfer (inside the PCM box) due to conduction only has been considered in these studies. Kibria et al. [15] have proposed an implicit scheme to model the heat balance. It is found that the mismatch of the computed values of the PV temperature from the experimental measurements remains within ± 3 °C. Brano et al. [16] have used a finite difference approach for the modelling and found a mismatch of ± 7 °C with that of the measured values.

* Corresponding authors.
*E-mail addresses:* s.khanna@exeter.ac.uk (S. Khanna), t.k.mallick@exeter.ac.uk (T.K. Mallick).

https://doi.org/10.1016/j.enconman.2018.04.056
Received 31 January 2018; Received in revised form 20 March 2018; Accepted 14 April 2018
Available online 03 May 2018
0196-8904/ © 2018 The Authors. Published by Elsevier Ltd. This is an open access article under the CC BY license (http://creativecommons.org/licenses/BY/4.0/).

**Nomenclature**

| | |
|---|---|
| $a_i$ | coefficients of polynomial in Eq. (29) |
| $C_p$ | heat capacity (J/kg K) |
| $D$ | function used to distribute the latent heat in phase change zone |
| $f$ | liquid fraction of the phase change material during phase transition |
| $F$ | view factor |
| $g$ | gravitational acceleration ($m^2/s$) |
| $G$ | portion of solar irradiance converted into heat ($W/m^3$) |
| $h$ | heat transfer coefficient due to convection ($W/m^2 K$) |
| $I_T$ | instantaneous solar-irradiance on tilted plane ($W/m^2$) |
| $k$ | thermal conductivity (W/m K) |
| $L$ | system length (m) |
| $L_h$ | heat capacity as latent (J/kg) |
| $p$ | pressure (Pa) |
| $s_f$ | spacing between fins (m) |
| $t$ | time (s) |
| $t_f$ | fin thickness (m) |
| $T$ | temperature (K) |
| $T_m$ | melting temperature of phase change material (K) |
| $u$ | velocity of phase change material (m/s) |

*Greek symbols*

| | |
|---|---|
| $\beta$ | tilt angle of the system (rad) |
| $\beta_c$ | coefficient for expansion of phase change material due to temperature (/K) |
| $\delta$ | depth of the PCM box (m) |
| $\varepsilon$ | emissivity for long wavelength radiation |
| $\eta_{PV}$ | PV efficiency |
| $\mu$ | dynamic viscosity (kg/ms) |
| $\rho$ | density ($kg/m^3$) |
| $\sigma$ | Stefan–Boltzmann constant ($W/m^2 K^4$) |

*Abbreviation*

| | |
|---|---|
| EVA | ethylene vinyl acetate |
| PCM | phase change material |
| PV | photovoltaic |

*Subscripts*

| | |
|---|---|
| a | ambient |
| al | aluminium |
| b | back of the PV |
| g | ground |
| i | $i^{th}$ layer of the PV |
| l | liquid phase |
| P | PCM |
| s | sky; solid phase |
| t | top surface |
| x | x direction |
| y | y direction |

Su et al. [17] have integrated the PCM and an air channel in their study for the thermal management of the PV and found an increment of 10.7% in the overall efficiency as compared to no-PCM case. Atkin and Farid [18] have integrated the PCM and the heat sink for PV cooling and reported an increment of 12.97% in the electrical output as compared to no-PCM and no-heat sink case.

The following studies have presented two dimensional thermal analyses of the PV-PCM system considering the heat transfer due to both conduction and convection inside the PCM box since convection affects the performance of the system significantly [19]. Huang et al. [20] have introduced aluminium fins inside the PCM box to enhance the PV cooling and found a further reduction of 3 °C in the PV temperature. Khanna et al. [21–24] have investigated the performance of the system for various operating conditions and optimized the quantity of PCM for PV-PCM and Finned-PV-PCM systems. Ho et al. [25] have proposed the encapsulation of the PCM at micro level. Huang [26] has studied the effect of the use of multiple PCMs on the cooling of the PV. The PCM changes its properties during phase transition zone and, thus, Biwole et al. [27] have presented the expressions to incorporate these changes.

Ho et al. [28,29] have used a three dimensional (3-d) model to study the conduction heat transfer in the system and reported the thermal management of the PV for southern Taiwan climate. Liu et al. [30] have used 3-d model by incorporating the heat transfer due to convection and reported that the PV temperature can be reduced further by 4 °C using PCM instead of water for a day in summer at Nanjing. Huang et al. [31,32] have reported that the mismatch between the temperature values computed using 2-d and 3-d models lies within −4 °C to 2 °C.

Apart from PV cooling, there have been studies analysing the performance of PCM for other purposes: Esen and Ayhan [33] have analysed the variation of stored energy with time for various types of phase change materials for a solar assisted energy storage tank. CCHH, Paraffin, SSDH and P-Wax have been considered as PCMs. Esen et al. [34] have carried out the optimization of the storage tank. Esen [35] has analysed the PCM storage tank integrated with solar powered heat pump system. Baby and Balaji [36] have studied the PCM based heat sink for the cooling of the portable electronic devices. Srikanth and Balaji [37] have carried out the optimization of the heat sink to achieve maximum charging period and minimum discharging period.

Thus, in literature, it is found that the researchers have reported the performance of the PV-PCM system for their respective locations. However, selection criteria for the climates suitable for PCM integration are not reported yet. Thus, in the current work, various types of climates have been chosen. The objectives of the presented study are (i) to present a mathematical model for analysing the transient behaviour of the system incorporating the effect of climate, (ii) to compute the decrease in the PV temperature achieved by the cooling of PV, (iii) to compute the increment in the electricity generation achieved by the PV cooling and (iv) to compare various climates in terms of the performance enhancement achieved by PCM integration. The performance enhancements have been compared for (i) the climate having less variations in the ambient temperature with that of the climate having large variations, (ii) warm climates with that of cold climates, (iii) climate with high wind speed with that of the climate having low wind speed, (iv) climate with high wind azimuth with that of the climate having low wind azimuth and (v) climate with high solar radiation with that of the climate having low solar radiation.

## 2. Methodology

The systems considered for the presented work are shown in Fig. 1. First system is only-PV panel. Second system consists of a PV attached with an aluminium box containing PCM. Third system considers aluminium fins inside the PCM box. All the systems are considered to be

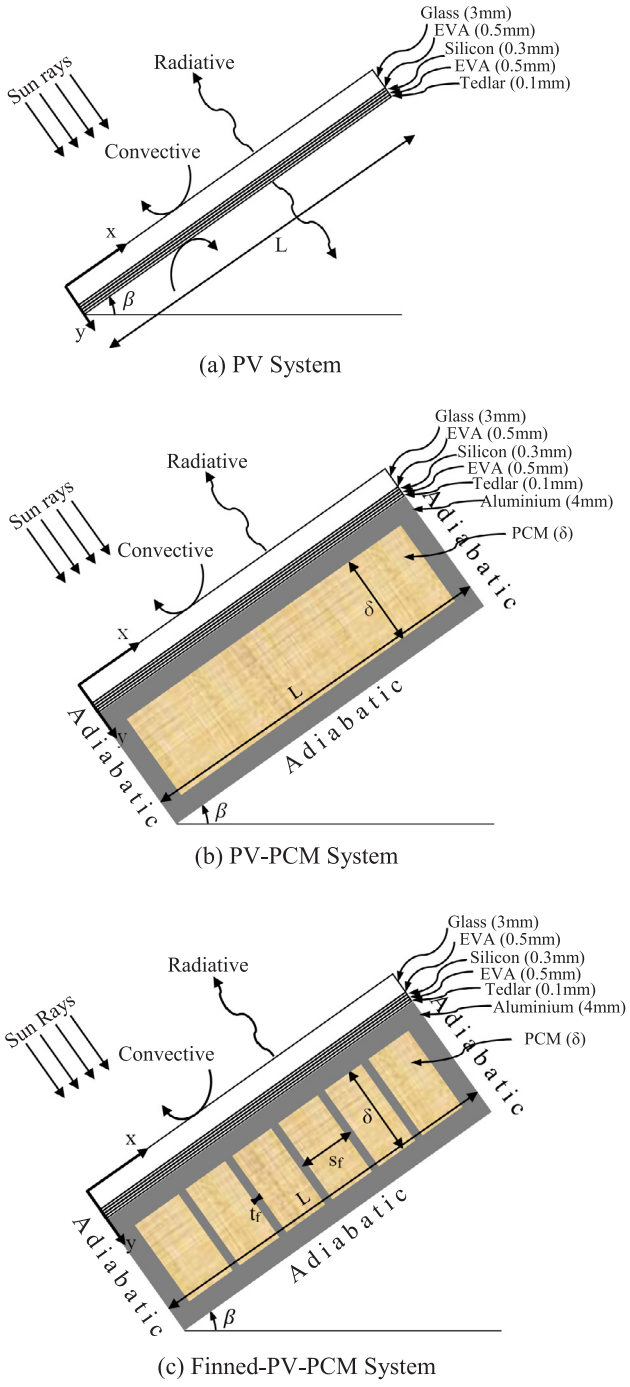


**Fig. 1.** Systems chosen for the presented study.

tilted at an angle $\beta$. Construct of the PV panel is considered to be a stack of five layers. $L$ and $\delta$ denote the length and depth of the PCM container. $s_f$ and $w_f$ denote the spacing and width of the fins.

The study is based on the assumptions given below

(i) The distribution of the solar flux on the surface of the PV is uniform
(ii) Heat loss from the bottom and the sides of the system is nil as thermal insulation is applied
(iii) An isotropic and homogeneous PV is considered for the study
(iv) The thermal properties of the PV are considered to be independent of temperature. However, variation in the efficiency is considered
(v) The PCM is considered to be isotropic and homogeneous in its solid and liquid phases
(vi) The thermal properties of the solid and liquid PCM are considered to be independent of temperature.

### 2.1. PV panel

To compute the thermal variations in the various layers of the PV in $x$ and $y$ directions at any time $t$, the following equation can be used

$$\rho_{PV,i} C_{p,PV,i} \frac{\partial T_{PV,i}}{\partial t} = G_i + k_{PV,i} \nabla^2 T_{PV,i} \tag{1}$$

with following boundary conditions

(a) The surfaces at $x = 0$ and $x = L$ experience nil rate of heat loss due to insulation. This boundary condition can be applied mathematically as follows

$$k_{PV,i} \frac{\partial T_{PV,i}}{\partial x}_{at\ x=0} = k_{PV,i} \frac{\partial T_{PV,i}}{\partial x}_{at\ x=L} = 0 \tag{2}$$

(b) The rate of heat leaving the surface at $y = 0$ is equal to the rate of heat transfer to surroundings due to convection and radiation. This boundary condition can be applied mathematically as follows

$$k_{PV} \frac{\partial T_{PV}}{\partial y}_{at\ y=0} = h_t [T_{PV,t} - T_a] + \sigma \varepsilon_t F_{t,s} [T_{PV,t}^4 - T_s^4] + \sigma \varepsilon_t F_{tg} [T_{PV,t}^4 - T_g^4] \tag{3}$$

(c) At any $i^{th}$ interface of PV layers, the rate of heat entering the $i^{th}$ PV layer from back is equal to the rate of heat leaving the $(i + 1)^{th}$ PV layer from front. This boundary condition can be applied mathematically as follows

$$k_{PV,i} \frac{\partial T_{PV,i}}{\partial y}_{at\ ith\ interface} = k_{PV,i+1} \frac{\partial T_{PV,i+1}}{\partial y}_{at\ ith\ interface} \tag{4}$$

(d) The rate of heat leaving from the back of the PV is equal to the rate of heat transfer to surroundings due to convection and radiation for PV system and is equal to the rate of heat entering the front surface of the aluminium container for PCM systems. This boundary condition can be applied mathematically as follows

For PV,

$$k_{PV,b} \frac{\partial T_{PV,b}}{\partial y} = h_b [T_{PV,b} - T_a] + \sigma \varepsilon_b F_{b,s} [T_{PV,b}^4 - T_s^4] + \sigma \varepsilon_b F_{bg} [T_{PV,b}^4 - T_g^4] \tag{5}$$

For PCM systems,

$$k_{PV,b} \frac{\partial T_{PV,b}}{\partial y} = k_{al,t} \frac{\partial T_{al,t}}{\partial y} \tag{6}$$

(e) Initially, the temperature of each $i^{th}$ layer of PV is equal to the ambient temperature. This boundary condition can be applied mathematically as follows

$$T_{PV,i_{at\ t=0}} = T_a \tag{7}$$

### 2.2. Aluminium box

The thermal variations in the aluminium box (at the back of the PV) in $x$ and $y$ directions at any time $t$ can be found out using the following equation

$$\rho_{al} C_{p,al} \frac{\partial T_{al}}{\partial t} = k_{al} \nabla^2 T_{al} \tag{8}$$

with following boundary conditions

(a) At the interfaces of aluminium and PCM, the rate of heat entering the PCM is equal to the rate of heat leaving the aluminium. These boundary conditions can be applied mathematically as follows

$$k_{al}\frac{\partial T_{al}}{\partial y} = k_P\frac{\partial T_P}{\partial y} \text{ at interfaces parallel to } x \text{ axis} \quad (9)$$

$$k_{al}\frac{\partial T_{al}}{\partial x} = k_P\frac{\partial T_P}{\partial x} \text{ at interfaces parallel to } y \text{ axis} \quad (10)$$

(b) The surfaces of the aluminium container at $x = 0$, $x = L$ and the back experience nil rate of heat loss due to insulation. These boundary conditions can be applied mathematically as follows

$$k_{al}\frac{\partial T_{al}}{\partial x}_{at\ x=0} = k_{al}\frac{\partial T_{al}}{\partial x}_{at\ x=L} = 0 \quad (11)$$

$$k_{al}\frac{\partial T_{al}}{\partial y} = 0 \text{ at back of container} \quad (12)$$

(c) Initially, the temperature of aluminium is equal to the ambient temperature. This boundary condition can be applied mathematically as follows

$$T_{al}{}_{at\ t=0} = T_a \quad (13)$$

### 2.3. PCM

To study the variations in the PCM in $x$ and $y$ directions at any time $t$, the following equations can be used

$$\rho_P C_{p,P}\frac{\partial T_P}{\partial t} = \nabla.(k_P\nabla T_P) - \frac{\partial}{\partial x}(\rho_P C_{p,P} u_x T_P) - \frac{\partial}{\partial y}(\rho_P C_{p,P} u_y T_P) \quad (14)$$

$$\rho_P\frac{\partial \vec{u}}{\partial t} + \rho_P(\vec{u}.\nabla)\vec{u} = -\frac{\partial p}{\partial x} + \mu\nabla^2\vec{u} + \rho_P\vec{g} \quad (15)$$

$$\nabla.\vec{u} = 0 \quad (16)$$

with following boundary conditions

(a) Inside the container, the velocity of the PCM is nil at all walls. This boundary condition can be applied mathematically as follows

$$u_x = u_y = 0 \text{ at all walls inside PCM container} \quad (17)$$

(b) Initially, the PCM velocity is nil and the temperature is same as that of the ambient.

$$u_{x,t=0} = u_{y,t=0} = 0 \quad (18)$$

$$T_{P}{}_{at\ t=0} = T_a \quad (19)$$

Eq. (14) conveys the conservation of energy, Eq. (15) conveys the conservation of momentum and Eq. (16) conveys the continuity. In Eq. (15), $\rho_P\vec{g}$ stands for the buoyancy force as follows

$$\rho_P\vec{g} = \rho_{P,l}[1-\beta_c(T_P-T_m)]\vec{g} \quad (20)$$

The sudden change in the thermal properties of the PCM during phase change must be handled delicately for the convergence and can be given as follows [27]

For the portions of PCM having temperature lesser than $T_{P,s}$,

$$C_{p,P}(T) = C_{p,P,s} \quad (21)$$

$$\rho_P(T) = \rho_{P,s} \quad (22)$$

$$k_P(T) = k_{P,s} \quad (23)$$

For the portions of the PCM during phase change,

$$C_{p,P}(T) = C_{p,P,s} + (C_{p,P,l}-C_{p,P,s})f(T) + L_h D(T) \quad (24)$$

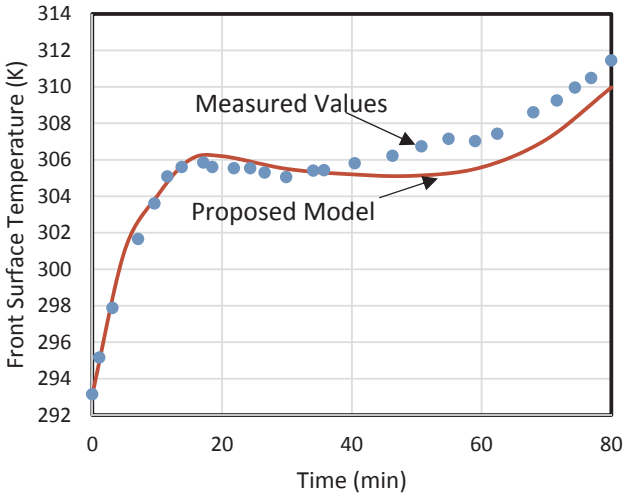


**Fig. 2a.** Validation against the experimental measurements [32].

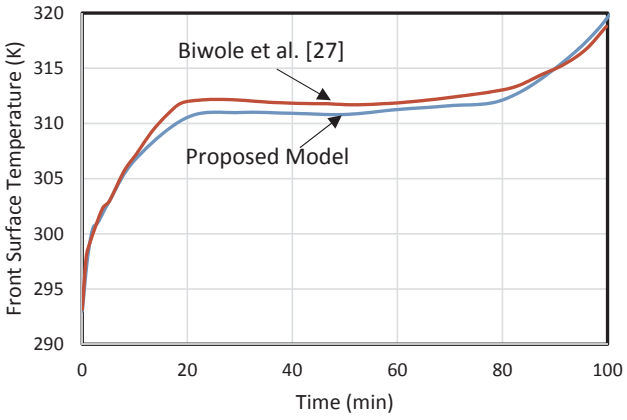


**Fig. 2b.** Validation against the results reported by Biwole et al. [27].

**Table 1**
Properties of different layers of PV and aluminium.

| Material | Thermal conductivity (W/m K) | Heat capacity (kJ/kg K) | Density (kg/m$^3$) | Thickness (mm) |
|---|---|---|---|---|
| Glass | 1.8 | 0.5 | 3000 | 3 |
| EVA | 0.35 | 2.1 | 960 | 0.5 |
| Silicon | 148 | 0.68 | 2330 | 0.3 |
| Tedlar | 0.2 | 1.25 | 1200 | 0.1 |
| Aluminium | 211 | 0.9 | 2675 | 4 |

$$\rho_P(T) = \rho_{P,s} + (\rho_{P,l}-\rho_{P,s})f(T) \quad (25)$$

$$k_P(T) = k_{P,s} + (k_{P,l}-k_{P,s})f(T) \quad (26)$$

For the portions of PCM having temperature greater than $T_{P,l}$

$$C_{p,P}(T) = C_{p,P,l} \quad (27)$$

$$\rho_P(T) = \rho_{P,l} \quad (28)$$

$$k_P(T) = k_{P,l} \quad (29)$$

where $C_{p,P,s}$, $C_{p,P,l}$, $\rho_{P,s}$, $\rho_{P,l}$, $k_{P,s}$ and $k_{P,l}$ are the heat capacities, densities and thermal conductivities of the PCM in solid and liquid phases respectively. $T_{P,s}$ and $T_{P,l}$ are the respective solidification and liquidification temperatures of the PCM. $L_h$ is the latent heat capacity of the PCM. $f(T)$ is the liquid fraction of the PCM for which a 2$^{nd}$ order continuous and differentiable function is defined (to ensure the

**Table 2**
Properties of RT 25 HC phase change material and other variables.

| Parameter | Value |
|---|---|
| $C_{p,P,s}$ (kJ/kg K) | 1.8 |
| $C_{p,P,l}$ (kJ/kg K) | 2.4 |
| $k_{P,s}$ (W/m K) | 0.19 |
| $k_{P,l}$ (W/m K) | 0.18 |
| $L$ (m) | 1 |
| $L_h$ (kJ/kg) | 232 |
| $s_f$ (cm) | 25 |
| $t_f$ (mm) | 4 |
| $T_{P,s}$ (°C) | 25.6 |
| $T_{P,l}$ (°C) | 27.6 |
| $\beta$ (°) | 45 |
| $\beta_c$ ($K^{-1}$) | 0.001 |
| δ (cm) | 5 |
| $\varepsilon$ | 0.85 |
| $\eta_{PV}$ (%) | $20[1-0.005(T_{PV}-25) + 0.085 \ln (I_T/1000)]$ |
| $\mu_s$ (kg/m s) | $10^5$ |
| $\mu_l$ (kg/m s) | 0.001798 |
| $\rho_{P,s}$ ($kg/m^3$) | 785 |
| $\rho_{P,l}$ ($kg/m^3$) | 749 |

convergence) by Biwole et al. [27] as follows

$$f(T) = \sum_{i=0}^{6} a_i T^i \tag{30}$$

with following boundary conditions

$$f_{at\ T_{P,s}} = \frac{df}{dT}_{at\ T_{P,s}} = \frac{d^2f}{dT^2}_{at\ T_{P,s}} = \frac{df}{dT}_{at\ T_{P,l}} = \frac{d^2f}{dT^2}_{at\ T_{P,l}} = 0,$$
$$f_{at\ T_{P,l}} = 1, f_{at\ T_m} = \frac{1}{2} \tag{31}$$

Using the above, the coefficients ($a_i$) can be given by

$$\begin{bmatrix} a_0 \\ a_1 \\ a_2 \\ a_3 \\ a_4 \\ a_5 \\ a_6 \end{bmatrix} = \begin{bmatrix} 1 & T_{P,s} & T_{P,s}^2 & T_{P,s}^3 & T_{P,s}^4 & T_{P,s}^5 & T_{P,s}^6 \\ 0 & 1 & 2T_{P,s} & 3T_{P,s}^2 & 4T_{P,s}^3 & 5T_{P,s}^4 & 6T_{P,s}^5 \\ 0 & 0 & 2 & 6T_{P,s} & 12T_{P,s}^2 & 20T_{P,s}^3 & 30T_{P,s}^4 \\ 0 & 1 & 2T_{P,l} & 3T_{P,l}^2 & 4T_{P,l}^3 & 5T_{P,l}^4 & 6T_{P,l}^5 \\ 0 & 0 & 2 & 6T_{P,l} & 12T_{P,l}^2 & 20T_{P,l}^3 & 30T_{P,l}^4 \\ 1 & T_{P,l} & T_{P,l}^2 & T_{P,l}^3 & T_{P,l}^4 & T_{P,l}^5 & T_{P,l}^6 \\ 1 & T_m & T_m^2 & T_m^3 & T_m^4 & T_m^5 & T_m^6 \end{bmatrix}^{-1} \begin{bmatrix} 0 \\ 0 \\ 0 \\ 0 \\ 0 \\ 1 \\ 0.5 \end{bmatrix} \tag{32}$$

For the section of the PCM where temperature is less than $T_{P,s}$, a very high viscosity has been taken to deal that portion as solid and the section for which temperature is above $T_{P,l}$, a very low viscosity has been taken. D(T) function (in Eq. (24)) is defined to spread the latent heat in the transition zone and can be given as follows

$$D(T) = \frac{e^{-(T-T_m)^2/[(T_{P,l}-T_{P,s})/4]^2}}{\sqrt{\pi\,[(T_{P,l}-T_{P,s})/4]^2}} \tag{33}$$

## 3. Solution method

The geometries of the systems have been built using ANSYS Fluent 17.1. Separate bodies for each layer of the systems (Glass, EVA, Silicon, EVA, Tedlar, Aluminium, Fins and PCM) have been generated. In order to incorporate the thin layers, mesh has been generated separately for each layer of the system by using 'Edge Sizing' in which each edge has been selected separately and number of divisions have been assigned to generate the nodes. In this way, a quadrilateral mesh has been generated. To model the interfaces, the nodes at the contact surfaces of two bodies are linked together using the energy balances. The interfaces of the bodies have been coupled to construct the complete systems. The boundary conditions have been applied on each wall of the geometry.

Pressure based solver is used to solve the equations. 'PRESTO' discretization method is chosen for pressure and 'First Order Upwind' for energy and momentum. The 'SIMPLE' scheme is used for Pressure-Velocity coupling.

Mesh independence study has been carried out. It is found that the increase in the number of nodes in the grid from $2.5 \times 10^4$ to $5 \times 10^4$ and $5 \times 10^4$ to $10 \times 10^4$ leads to the change in the PV temperature by 0.49% and 0.06% respectively. Keeping the selection criterion of change to be lesser than 0.1%, number of nodes in the grid is chosen as $5 \times 10^4$.

It is found that the decrease in the time step from 1 s to 0.5 s, 0.5 s to 0.25 s, 0.25 s to 0.1 s and 0.1 s to 0.05 s leads to change in the PV temperature by 3.2%, 1.3%, 0.6% and 0.08% respectively. Keeping the selection criterion of change to be lesser than 0.1%, time step is chosen as 0.1 s. Similarly, the values of energy, velocity and continuity acceptable residuals are chosen as $10^{-8}$, $10^{-4}$ and $10^{-4}$ respectively. For the chosen parameters, the software take 10 real seconds for the simulations of 1 s using 24 GB of RAM and Intel (R) Xenon (R) CPU.

## 4. Verification

For the validation of the proposed model with the experimental study, the measurements taken by Huang et al. [32] have been considered. In their study, RT 25 HC PCM was used. The values of $I_T$ and $T_a$ were 750 W/$m^2$ and 20 °C respectively. The side walls of the system were insulated. Using the equations, the calculations have been carried out for similar system. The front-surface temperature has been shown in Fig. 2a along with the experimental values. It is observed that the mismatch between the estimated results and the reported ones lies between −0.6% to +0.2%. The mismatch is due to the fact that the proposed model incorporates all the latent heat within a specified temperature zone. However, in reality, some fraction of the latent heat is also spread beyond the temperature zone chosen for the calculations. Thus, during the absorption of latent heat, the mismatch is higher.

For the verification of the proposed model with the results reported by Biwole et al. [27], the calculations have been carried out for similar system. In their study, RT 25 HC PCM was used. The values of $I_T$ and $T_a$ were 1000 W/$m^2$ and 20 °C respectively. The side walls of the system were insulated. Both the calculated and the reported results of the front-surface temperature are shown in Fig. 2b. It is observed that the mismatch between the estimated results and the reported ones lies between ± 0.5%.

## 5. Results and discussion

In the presented work, the variations in the temperature and the electricity generation from the systems with time have been computed for various types of climates. The increment in the electricity generation achieved by the cooling of PV have also been compared. The source [38] of the climate data provides the values with time interval of 15 min. The physical and thermal properties of the PV and PCM are listed in Tables 1 and 2. RT 18 HC, RT 25 HC and RT 35 HC [39] have been taken as PCM according to the range of the ambient temperature of the corresponding climate.

### 5.1. Climates with large/less variations in ambient temperature

The PV temperature and the electricity generation from the systems are computed for climates having large variations in ambient temperature (Madrid, 40.4°N 3.7°W) and less variations (Benidorm, 38.5°N 0.1°W) (Fig. 3a) and presented in Fig. 3b–f.

The results show that, near noon, the PV temperature is decreased from 60.1 °C to 41.8 °C (Fig. 3b) and 60.1 °C to 38.5 °C (Fig. 3c) using PCM systems for the climate having large variations and from 58.8 °C to 36.2 °C (Fig. 3b) and 58.8 °C to 32.9 °C (Fig. 3c) for the climate having less variations. The corresponding electrical output is increased from 164.9 W/$m^2$ to 181.2 W/$m^2$ (Fig. 3d) and 164.9 W/$m^2$ to 184.5 W/$m^2$

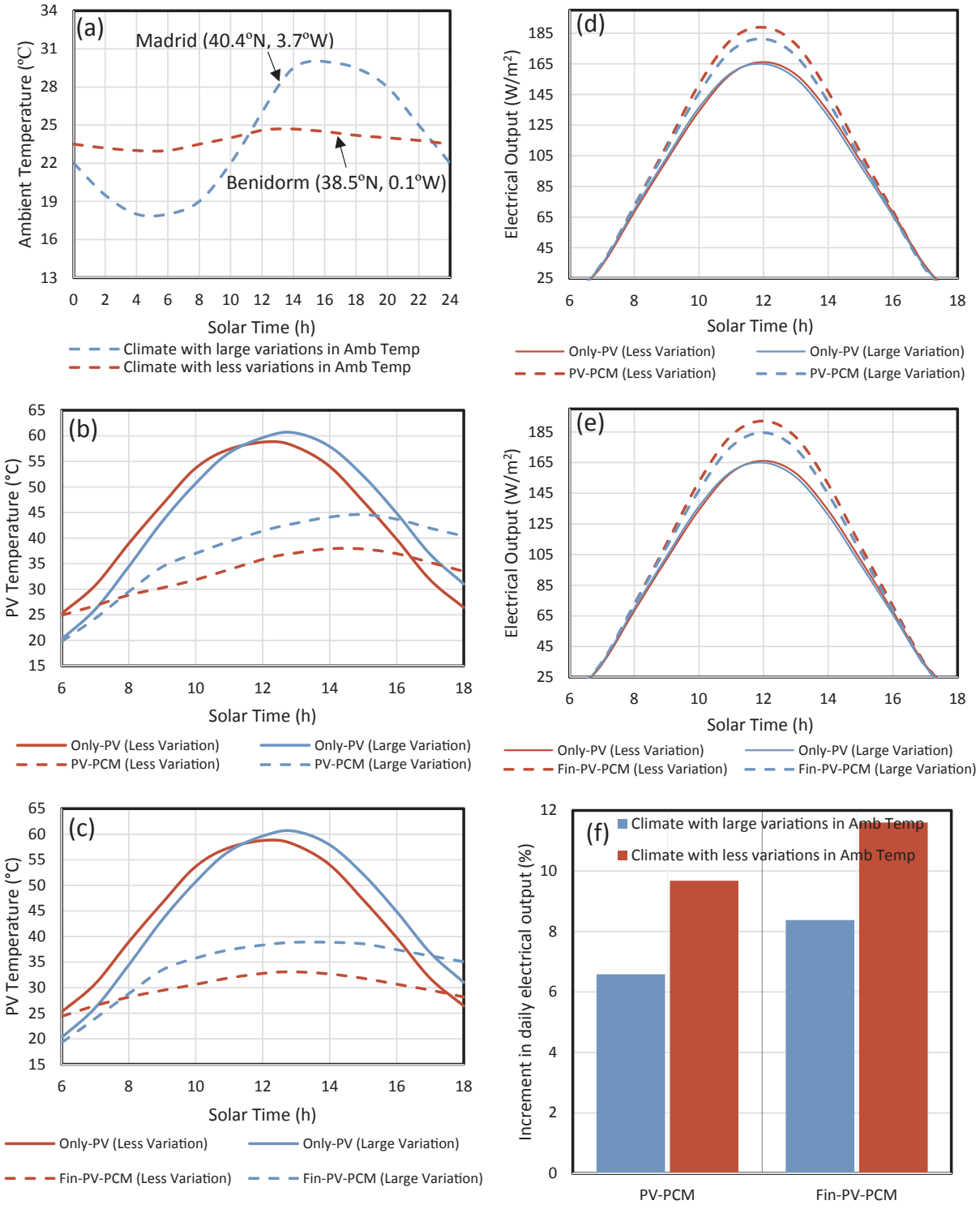


**Fig. 3.** PV temperature and electricity generation from systems for climates having large/less variations in ambient temperature.

(Fig. 3e) using PCM systems for the climate having large variations and from 166.1 W/m$^2$ to 188.8 W/m$^2$ (Fig. 3d) and 166.1 W/m$^2$ to 192.1 W/m$^2$ (Fig. 3e) for the climate having less variations.

The results show that the daily electricity enhancements are 6.6% and 8.4% (Fig. 3f) using PCM systems for the climate having large variations which increase to 9.7% and 11.6% (Fig. 3f) for the climate with less variations (Fig. 3d).

Thus, if the ambient temperature varies a lot over day/month, the PCM integration is less effective. It is due to the fact that if the ambient temperature becomes higher than the PCM melting temperature for some days/months, the PCM will remain melted for that duration and cannot extract much heat from the PV. If PCM with higher melting temperature is chosen according to the upper limit of the ambient temperature, even then, it cannot extract heat from PV effectively because PCM extracts most of the heat (as latent heat) during phase change near to its melting temperature which is higher in this case.

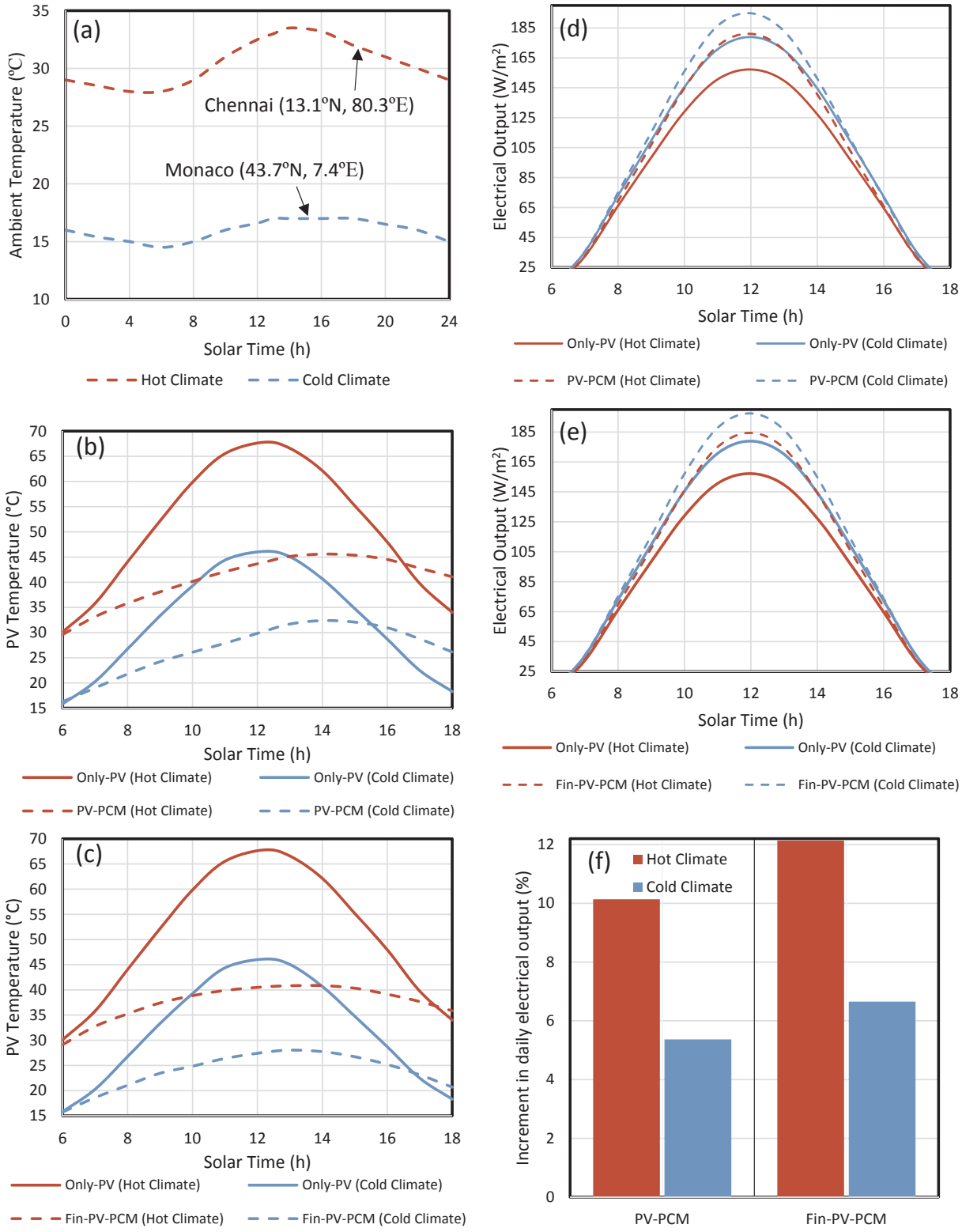


**Fig. 4.** PV temperature and electricity generation from systems for hot and cold climates.

### 5.2. Comparison of hot and cold climates

The PV temperature and the electricity generation from the systems are computed for hot (Chennai, 13.1°N 80.3°E) and cold (Monaco, 43.7°N 7.4°E) climates (Fig. 4a) and presented in Fig. 4b–f.

The results show that, near noon, the PV temperature is decreased from 46.1 °C to 30.2 °C (Fig. 4b) and 46.1 °C to 27.6 °C (Fig. 4c) using PCM systems for the cold climate and from 67.7 °C to 44.0 °C (Fig. 4b) and 67.7 °C to 40.6 °C (Fig. 4c) for the hot climate. The corresponding electrical output is increased from 178.9 W/m$^2$ to 194.8 W/m$^2$ (Fig. 4d) and 178.9 W/m$^2$ to 197.4 W/m$^2$ (Fig. 4e) using PCM systems for the cold climate and from 157.2 W/m$^2$ to 181.0 W/m$^2$ (Fig. 4d) and 157.2 W/m$^2$ to 184.4 W/m$^2$ (Fig. 4e) for the hot climate.

The results show that the daily electricity enhancements are 5.3%

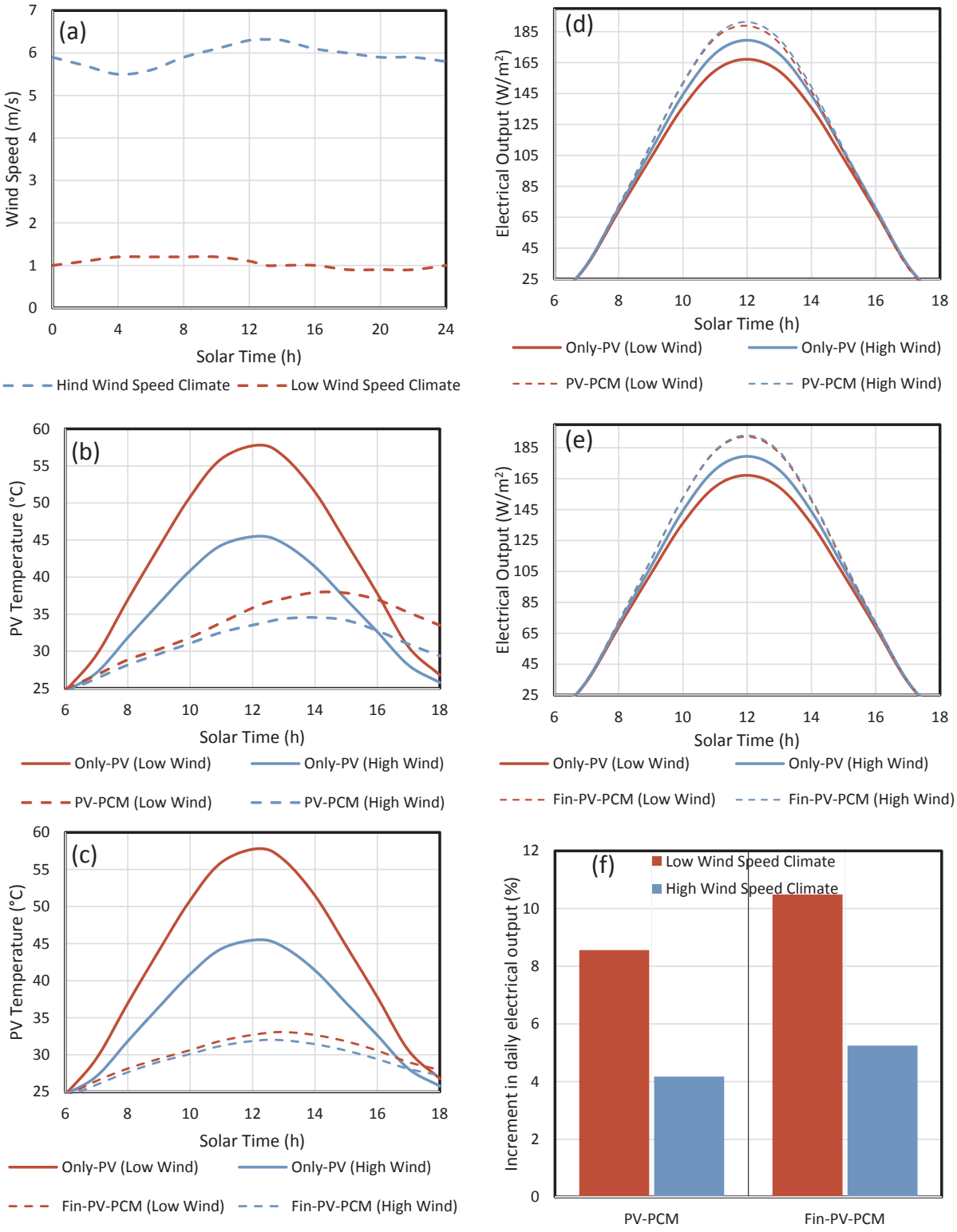


**Fig. 5.** PV temperature and the electricity generation from systems for climates having different wind speed.

and 6.6% (Fig. 4f) using PCM systems for the cold climate which increase to 10.0% and 12.1% (Fig. 4f) for the hot climate.

Thus, for the cold climate, the PCM integration is less effective. It is due to the fact that the low ambient temperature itself maintains the PV at lower temperatures which reduces the rate of heat transfer from PV to PCM. Thus, PCM cannot extract much heat from PV in cold climates.

### 5.3. Comparison of climates having different wind speeds

The PV temperatures in the systems are computed for different climates having different wind speeds (Fig. 5a) and presented in Fig. 5b–c. The corresponding electricity generations from the systems are presented in Fig. 5d–f.

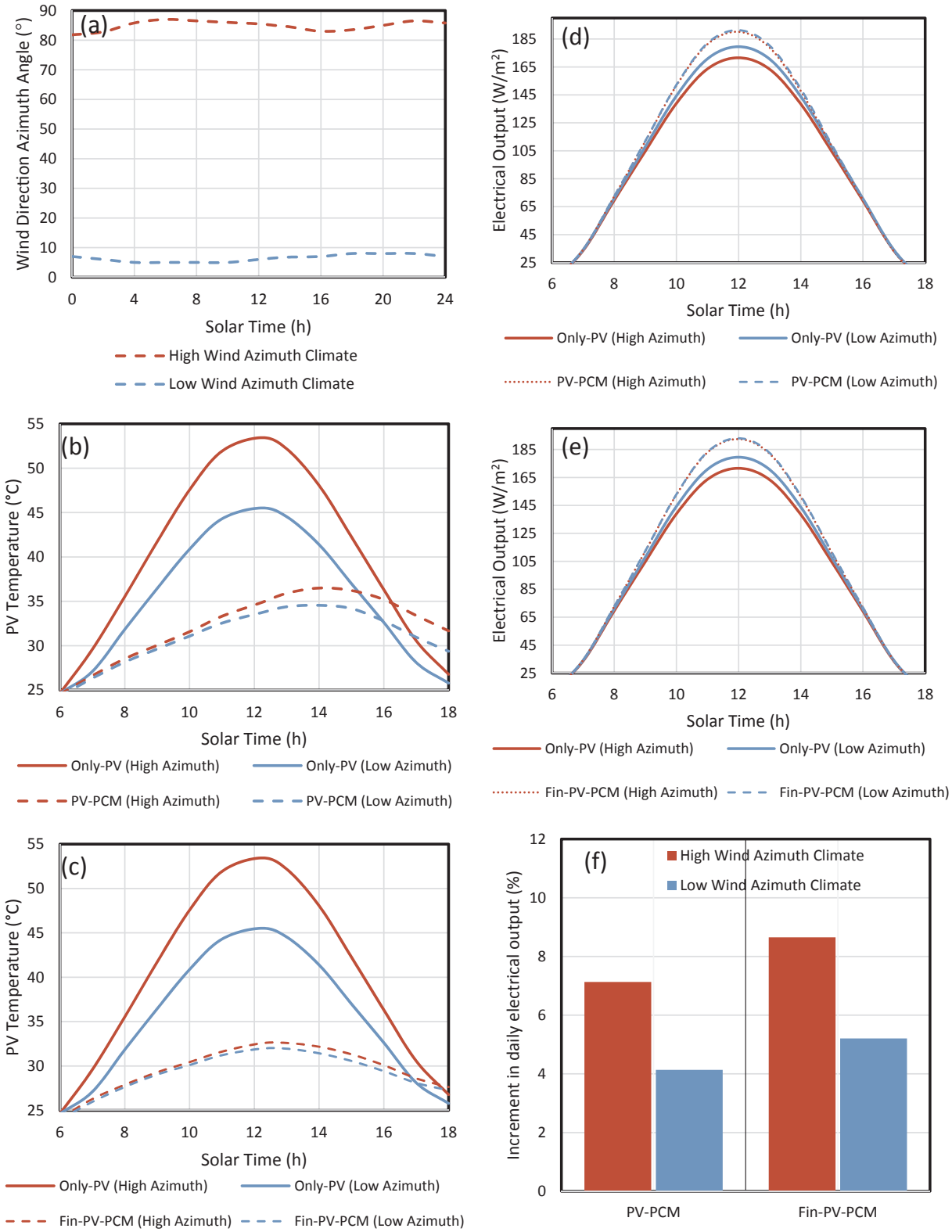


**Fig. 6.** PV temperature and the electricity generation from systems for climates having different wind-directions.

The results show that, near noon, the PV temperature is decreased from 45.5 °C to 33.7 °C (Fig. 5b) and 45.5 °C to 31.9 °C (Fig. 5c) using PCM systems for location having high wind speed and from 57.8 °C to 36.2 °C (Fig. 5b) and 57.8 °C to 32.8 °C (Fig. 5c) for location having low wind speed. The corresponding electrical output is increased from 179.5 W/m$^2$ to 191.3 W/m$^2$ (Fig. 5d) and 179.5 W/m$^2$ to 193.1 W/m$^2$ (Fig. 5e) using PCM systems for location having high wind speed and from 167.2 W/m$^2$ to 188.9 W/m$^2$ (Fig. 5d) and 167.2 W/m$^2$ to 192.2 W/m$^2$ (Fig. 5e) for location having low wind speed.

The results show that for location having high wind speed, the daily electricity enhancements are 4.1% and 5.2% (Fig. 5f) using PCM systems which increase to 8.5% and 10.4% (Fig. 5f) for location having low wind speed.

Thus, the PCM integration is less effective in high wind speeds. It is

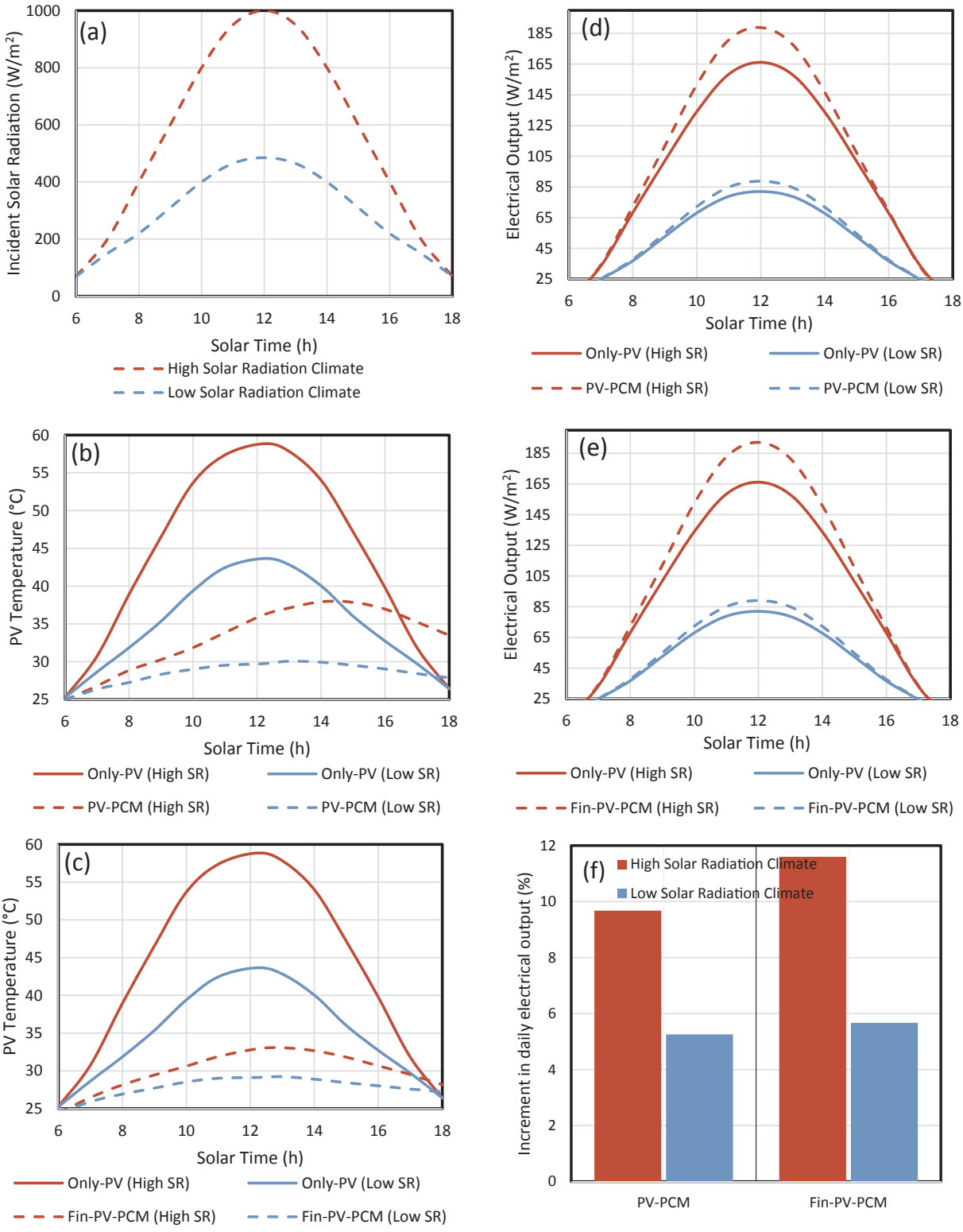


**Fig. 7.** PV temperature and the electricity generation from systems for climates having different solar radiation availability.

due to the fact that the higher wind speed cools down the PV to a certain level without using PCM. It reduces the contribution of PCM in PV cooling for locations having high wind speed.

### 5.4. Comparison of climates having different wind-directions

The PV temperatures in the systems are computed for different climates having different wind-directions (Fig. 6a) and presented in Fig. 6b–c. The corresponding electricity generation from the systems are presented in Fig. 6d–f.

The results show that, near noon, the PV temperature is decreased from 53.4 °C to 34.8 °C (Fig. 6b) and 53.4 °C to 32.5 °C (Fig. 6c) using PCM systems for location having wind-flow across the PV and from 45.5 °C to 33.7 °C (Fig. 6b) and 45.5 °C to 31.9 °C (Fig. 6c) for location

having wind-flow normal to the PV. The corresponding electrical output is increased from 171.6 W/m$^2$ to 190.2 W/m$^2$ (Fig. 6d) and 171.6 W/m$^2$ to 192.5 W/m$^2$ (Fig. 6e) using PCM systems for location having wind-flow across the PV and from 179.5 W/m$^2$ to 191.3 W/m$^2$ (Fig. 6d) and 179.5 W/m$^2$ to 193.0 W/m$^2$ (Fig. 6e) for location having wind-flow normal to the PV.

The results show that for location having wind-flow across the PV, the daily electricity enhancements are 7.1% and 8.6% (Fig. 6f) using PCM systems which become 4.1% and 5.2% (Fig. 6f) for location having wind-flow normal to the PV.

Thus, the results show that for the locations where wind flows normal to the PV, the PCM integration is less effective. It is due to the fact that when wind-flow is normal to the PV, the heat losses from PV are higher which maintain the PV at lower temperatures and, thus, leads to lesser scope of further lowering down the PV temperature using PCM.

### 5.5. Climates with different solar radiation availability

The PV temperature and the electricity generation from the systems are computed for different climates having different solar radiation availability (Fig. 7a) and presented in Fig. 7b–f. The results show that the increments in the electricity generation are 9.7% and 11.6% (Fig. 7f) using PCM systems for the location having high solar radiation which reduce to 5.2% and 5.7% (Fig. 7f) for the one with low solar radiation.

Thus, the PCM integration is more effective for the locations having high solar radiation. It is due to the fact that for low solar radiation, the heat generation inside the PV is lesser which reduces the rate of heat extraction by PCM from the PV.

## 6. Conclusions

In the current work, mathematical model has been presented to study the effect of climate on the performance of photovoltaic (PV) integrated with phase change material (PCM). The variations in the temperature and electricity generation from the systems with time have been computed for various types of climates. The corresponding increments in the electricity generation achieved by the cooling of PV have also been computed. The following conclusions are found out.

(i) The electricity enhancement is 9.7% for the climate having less variations in ambient temperature. However, it reduces to 6.6% for the climate having large variations in the ambient temperature.
(ii) Cold climates are less suitable for heat extraction by PCM from PV. The electricity enhancement is 5.3% for the cold climate which increase to 10.0% for warm climate.
(iii) PCM integration with PV performs better in climates having low wind speed (in terms of PCM contribution in PV cooling). The electricity enhancement is 8.5%. It reduces to 4.1% for climate having high wind speed.
(iv) PV cooling using phase change material is more effective for the climate where wind flow is across the system. The electricity enhancement is 7.1%.
(v) Climates having high solar radiation availability are better for PCM systems. In these climates, these systems can yield 9.7% higher electricity generation as compared to PV system.

## Acknowledgment

The authors gratefully acknowledge the financial support from EPSRC-DST funded Reliable and Efficient System for Community Energy Solution - RESCUES project (EP/K03619X/1). In support of open access research, all underlying article materials (such as data, samples or models) can be accessed upon request via email to the corresponding author.

## References

[1] Skoplaki E, Palyvos JA. On the temperature dependence of photovoltaic module electrical performance: a review of efficiency/power correlations. Sol Energy 2009;83:614–24.
[2] Hasan A, McCormack SJ, Huang MJ, Norton B. Evaluation of phase change materials for thermal regulation enhancement of building integrated photovoltaics. Sol Energy 2010;84:1601–12.
[3] Indartono YS, Suwono A, Pratama FY. Improving photovoltaics performance by using yellow petroleum jelly as phase change material. Int J Low-Carbon Technol 2014:1–5.
[4] Huang MJ, Eames PC, Norton B. Phase change materials for limiting temperature rise in building integrated photovoltaics. Sol Energy 2006;80:1121–30.
[5] Hasan A, McCormack SJ, Huang MJ, Sarwar J, Norton B. Increased photovoltaic performance through temperature regulation by phase change materials: materials comparison in different climates. Sol Energy 2015;115:264–76.
[6] Sharma S, Tahir A, Reddy KS, Mallick TK. Performance enhancement of a building-integrated concentrating photovoltaic system using phase change material. Sol Energy Mater Sol Cells 2016;149:29–39.
[7] Cui T, Xuan Y, Yin E, Li Q, Li D. Experimental investigation on potential of a concentrated photovoltaic-thermoelectric system with phase change materials. Energy 2017;122:94–102.
[8] Sardarabadi M, Passandideh-Fard M, Maghrebi M, Ghazikhani M. Experimental study of using both ZnO/water nanofluid and phase change material (PCM) in photovoltaic thermal systems. Sol Energy Mater Sol Cells 2017;161:62–9.
[9] Browne MC, Lawlor K, Kelly A, Norton B, McCormack SJ. Indoor characterisation of a photovoltaic/thermal phase change material system. Energy Proc 2015;70:163–71.
[10] Huang MJ, Eames PC, Norton B, Hewitt NJ. Natural convection in an internally finned phase change material heat sink for the thermal management of photovoltaics. Sol Energy Mater Sol Cells 2011;95:1598–603.
[11] Browne MC, Norton B, McCormack SJ. Phase change materials for photovoltaic thermal management. Renew Sustain Energy Rev 2015;47:762–82.
[12] Ma T, Yang H, Zhang Y, Lu L, Wang X. Using phase change materials in photovoltaic systems for thermal regulation and electrical efficiency improvement: a review and outlook. Renew Sustain Energy Rev 2015;43:1273–84.
[13] Du D, Darkwa J, Kokogiannakis G. Thermal management systems for Photovoltaics (PV) installations: a critical review. Sol Energy 2013;97:238–54.
[14] Shukla A, Kant K, Sharma A, Biwole PH. Cooling methodologies of photovoltaic module for enhancing electrical efficiency: a review. Sol Energy Mater Sol Cells 2017;160:275–86.
[15] Kibria MA, Saidur R, Al-Sulaiman FA, Aziz MMA. Development of a thermal model for a hybrid photovoltaic module and phase change materials storage integrated in buildings. Sol Energy 2016;124:114–23.
[16] Brano VL, Ciulla G, Piacentino A, Cardona F. Finite difference thermal model of a latent heat storage system coupled with a photovoltaic device: description and experimental validation. Renew Energy 2014;68:181–93.
[17] Su D, Jia Y, Alva G, Liu L, Fang G. Comparative analyses on dynamic performances of photovoltaic–thermal solar collectors integrated with phase change materials. Energy Convers Manage 2017;131:79–89.
[18] Atkin P, Farid MM. Improving the efficiency of photovoltaic cells using PCM infused graphite and aluminium fins. Sol Energy 2015;114:217–28.
[19] Kant K, Shukla A, Sharma A, Biwole PH. Heat transfer studies of photovoltaic panel coupled with phase change material. Sol Energy 2016;140:151–61.
[20] Huang MJ, Eames PC, Norton B. Thermal regulation of building-integrated photovoltaics using phase change materials. Int J Heat Mass Transf 2004;47:2715–33.
[21] Khanna S, Reddy KS, Mallick TK. Performance analysis of tilted photovoltaic system integrated with phase change material under varying operating conditions. Energy 2017;133:887–99.
[22] Khanna S, Sundaram S, Reddy KS, Mallick TK. Performance analysis of perovskite and dye-sensitized solar cells under varying operating conditions and comparison with monocrystalline silicon cell. Appl Therm Eng 2017;127:559–65.
[23] Khanna S, Reddy KS, Mallick TK. Optimization of solar photovoltaic system integrated with phase change material. Sol Energy 2018;163:591–9.
[24] Khanna S, Reddy KS, Mallick TK. Optimization of finned solar photovoltaic phase change material (Finned PV PCM) System; 2018 [submitted for publication].
[25] Ho CJ, Tanuwijava AO, Lai CM. Thermal and electrical performance of a BIPV integrated with a microencapsulated phase change material layer. Energy Build 2012;50:331–8.
[26] Huang MJ. The effect of using two PCMs on the thermal regulation performance of BIPV systems. Sol Energy Mater Sol Cells 2011;95:957–63.
[27] Biwole PH, Eclache P, Kuznik F. Phase-change materials to improve solar panel's performance. Energy Build 2013;62:59–67.
[28] Ho CJ, Chou WL, Lai CM. Thermal and electrical performance of a water-surface floating PV integrated with a water-saturated MEPCM layer. Energy Convers Manage 2015;89:862–72.
[29] Ho CJ, Chou WL, Lai CM. Application of a water-saturated MEPCM-PV for reducing winter chilling damage on aqua farms. Sol Energy 2014;108:135–45.
[30] Liu L, Jia Y, Lin Y, Alva G, Fang G. Numerical study of a novel miniature compound parabolic concentrating photovoltaic/thermal collector with microencapsulated phase change slurry. Energy Convers Manage 2017;153:106–14.
[31] Huang MJ, Eames PC, Norton B. Comparison of a small-scale 3D PCM thermal control model with a validated 2D PCM thermal control model. Sol Energy Mater Sol Cells 2006;90:1961–72.
[32] Huang MJ, Eames PC, Norton B. Comparison of predictions made using a new 3D

phase change material thermal control model with experimental measurements and predictions made using a validated 2D model. Heat Transfer Eng 2007;28:31–7.
[33] Esen M, Ayhan T. Development of a model compatible with solar assisted cylindrical energy storage tank and variation of stored energy with time for different phase-change materials. Energy Convers Manage 1996;37(12):1775–85.
[34] Esen M, Durmus A, Durmus A. Geometric design of solar-aided latent heat store depending on various parameters and phase change materials. Sol Energy 1998;62(1):19–28.
[35] Esen M. Thermal performance of a solar-aided latent heat store used for space heating by heat pump. Sol Energy 2000;69(1):15–25.
[36] Baby R, Balaji C. Experimental investigations on phase change material based finned heat sinks for electronic equipment cooling. Int J Heat Mass Transf 2012;55:1642–9.
[37] Srikanth R, Balaji C. Experimental investigation on the heat transfer performance of a PCM based pin fin heat sink with discrete heating. Int J Therm Sci 2017;111:188–203.
[38] Climate data < http://photovoltaic-software.com/pvgis.php > [accessed 22.08.2017].
[39] Rubitherm Phase Change Material < https://www.rubitherm.eu/ > [accessed 22.08.2017].